On the lattice site of trivalent dopants and the structure of Mg^{2+}-OH^{-}-M^{3+} defects in $LiNbO_3$:Mg crystals

1993 J. Phys.: Condens. Matter 5 781

(http://iopscience.iop.org/0953-8984/5/7/006)

J. Phys.: Condens. Matter 5 (1993) 781–794. Printed in the UK

On the lattice site of trivalent dopants and the structure of Mg^{2+}–OH^-–M^{3+} defects in $LiNbO_3$:Mg crystals

L Kovács†, L Rebouta‡, J C Soares‡, M F da Silva§, M Hage-Ali||, J P Stoquert||, P Siffert||, J A Sanz-García¶, G Corradi†, Zs Szaller† and K Polgár†

† Research Laboratory for Crystal Physics of the Hungarian Academy of Sciences, 1502 Budapest, PO Box 132, Hungary
‡ Centro de Física Nuclear da Universidade de Lisboa, 1699 Lisboa Codex, Portugal
§ Departamento de Física, ICEN, LNETI, 2685 Sacavém, Portugal
|| Laboratoire PHASE du CNRS, Centre de Recherches Nucléaires, 67037 Strasbourg, France
¶ Instituto de Ciencia de Materiales, CSIC and Departamento de Física Aplicada C-IV, Universidad Autónoma de Madrid, 28049 Madrid, Spain

Received 27 July 1992, in final form 6 November 1992

Abstract. The lattice sites of a number of trivalent co-dopants (In, Nd, Gd, Er, Tm, and Lu) have been determined in $LiNbO_3$ crystals doped also with Mg, using the Rutherford back-scattering and proton-induced x-ray emission channelling techniques. In, Er and Lu have been found mainly on Li sites, but a small fraction of In and Lu may substitute for Nb ions. Gd and Tm ions also replace mainly Li, but some of these ions seem to be present in other positions, possibly related to some kinds of aggregate, e.g. self-compensating pairs. A fraction of Nd ions probably occupies interstitial sites in structurally empty oxygen octahedra, while other Nd ions may substitute for host cations. In addition to the already known effect of Cr, Fe and Nd ions, In, Lu and also Sc give rise to an OH^- absorption band between 3499 and 3523 cm^{-1}, which is attributed to Mg^{2+}(Li site)–OH^-(O site)–M^{3+}(Nb site) complex defects. No such band is observed for Y, Gd, Er and Tm co-doped crystals.

1. Introduction

Lithium niobate ($LiNbO_3$) crystals are widely used in optical signal processing. Dopants have been found to influence the optical properties utilized in applications [1, 2]. For example Fe is generally used to increase the photorefractive response of the crystal, Ti in-diffusion creates a waveguiding layer, while Nd is a laser activator in the $LiNbO_3$ host matrix.

Knowledge of the lattice position of the impurities is indispensable for understanding the microscopic processes induced by the dopants. In the early papers it was generally assumed that tetravalent impurities occupy Nb^{5+} sites while divalent dopants substitute for Li^+, reducing the charge misfit as much as possible [3]. This assumption has recently been confirmed for Mn^{2+} by electron nuclear double resonance (ENDOR) [4] and extended x-ray absorption fine-structure (EXAFS) experiments [5] but has failed for Hf^{4+} which has also been found to replace Li in

0953-8984/93/070781+14$07.50

the lattice [6, 7]. Both divalent Ni^{2+} and tetravalent Ti^{4+} seem to occupy mainly Li sites as deduced from EXAFS data [8].

For trivalent impurities it was assumed that they may occur at both niobium and lithium lattice positions [3]. The lattice location of Cr^{3+} ions is still under discussion [9, 10]. Cr^{3+}–Cr^{3+} pairs, apparently occupying neighbouring lithium and niobium sites for charge compensation, were also identified, especially at high concentrations of chromium [11–13]. Fe^{3+} ions, however, substitute mainly for Li as was concluded from proton-induced x-ray emission (PIXE) [14] and EXAFS [15] experiments. Optical spectroscopy methods show that Eu^{3+} and Nd^{3+} ions occupy two different sites [16, 17]. By using the Rutherford back-scattering (RBS) channelling technique, Eu^{3+} and Nd^{3+} ions have recently been found to occupy lithium sites strongly shifted from the regular Li position towards the nearest oxygen plane [18]. It has to be mentioned that recent computer simulation studies predict the occupation of Li sites for both divalent and trivalent impurities, at least for low dopant concentrations [19].

$LiNbO_3$ is a non-stoichiometric material with an Li-deficient congruent composition (Li-to-Nb ratio, 0.94). It has been shown by x-ray diffraction experiments [20] and theoretical calculations [21] that the missing Li^+ ions are replaced by Nb^{5+} ions with compensating vacancies at the Nb sites. The number of antisite niobium atoms (Nb_{Li}) can be decreased by increasing the Li-to-Nb ratio or by adding Mg to the crystal [19, 22]. Magnesium has a great practical importance in reducing the photorefractive laser damage above a threshold concentration of about 4.6 at.% Mg in $LiNbO_3$ [23]. Mg ions incorporated in Li sites and reducing the number of Nb_{Li} ions may also influence the location of other impurities used to co-dope the crystal. It was shown by the RBS channelling technique that Hf^{4+} ions which occupy Li sites in $LiNbO_3$ without Mg substitute for Nb in crystals co-doped with Mg [18, 24]. New electron paramagnetic resonance (EPR) signals have been attributed to Cr^{3+} and Fe^{3+} impurities on Nb sites in Mg-co-doped $LiNbO_3$ [9, 25], with ENDOR proof in the Cr^{3+} case [9]. These signals are absent in crystals doped with only Cr^{3+} or Fe^{3+}. The optical spectra also suggest the presence of Cr^{3+} and Nd^{3+} ions on Nb sites with neighbouring Mg on the Li site in Mg-co-doped $LiNbO_3$ crystals [17, 26].

In addition to the above-mentioned methods, infrared (IR) absorption spectroscopy of hydroxyl ions can also provide some information about the structure of defects induced by non-stoichiometry and the dopants. The shape of the OH^- band at about 3485 cm^{-1} was found to be sensitive to the Li-to-Nb ratio of the undoped crystal [27]. Additional absorption bands appeared at about 3538 cm^{-1} in heavily Mg-doped $LiNbO_3$ [28, 29] and at about 3506 cm^{-1} and 3522 cm^{-1} in $LiNbO_3$: Mg co-doped with some transition-metal impurities (Cr and Fe) [30–32] and Nd [33], respectively. Since the 3506 cm^{-1} and 3522 cm^{-1} bands were found only in doubly doped crystals, they were assigned to OH^- related to an Mg–OH–M type of defect complex where Mg^{2+}, OH^- and M^{3+} trivalent dopant occupy Li, O and Nb sites, respectively, forming locally neutral complexes [30, 33].

In two recent short communications [34, 35] we presented some preliminary results on the lattice site of trivalent dopants in $LiNbO_3$:Mg. In the present paper we give a detailed description of the experiments and a larger set of the data obtained by the RBS and the PIXE channelling techniques. We shall also discuss the occurrence and the structure of the Mg^{2+}–OH^-–M^{3+} defects detected by the IR absorption spectroscopy of hydroxyl ions.

2. Experimental details

$LiNbO_3$ crystals were grown in air by the diameter-controlled Czochralski method either at the Research Laboratory for Crystal Physics, Budapest, or at the Departamento de Física Aplicada, Universidad Autónoma de Madrid. Each $LiNbO_3$ melt was doped with MgO simultaneously with the oxide of one of the following elements: Sc, Y, In, Nd, Gd, Er, Tm or Lu. The dopant concentrations in the melt and in the crystal as determined by atomic absorption spectroscopy (AAS) and inductively coupled plasma (ICP) methods are listed in tables 1 and 2.

Table 1. Concentrations of the dopants determined by the AAS or ICP methods and the positions of the OH absorption bands in Mg^{2+}-and-M^{3+}-co-doped $LiNbO_3$ crystals.

Spectrum in figure 7	Dopant	Mg concentration (mol%) Melt	Mg concentration (mol%) Crystal	Dopant concentration (mol%) Melt	Dopant concentration (mol%) Crystal	OH absorption wavenumber (cm^{-1})	Remark
A	Y	6	5	1	0.72	3495	Weak
						3528.1	Mg–OH
						3538.1	Mg–OH
B	Y	8		1		3491.4	Very weak
						3528.9	Mg–OH
						3538.4	Mg–OH
C	Er	6	4.8	1	0.79	3491.1	Weak
						3527.9	Mg–OH
						3538.3	Mg–OH
D	Er	8	7.5	1	0.57	3493.1	Very weak
						3527.4	Mg–OH
						3537.8	Mg–OH
E	Tm	6		1	0.4[a]	3492.2	Very weak
						3526.5	Mg–OH
						3536.8	Mg–OH
F	Gd	6		1	0.6[a]	3488.2	Very weak
						3526.3	Mg–OH
						3537.1	Mg–OH

[a] The concentration of the dopant was estimated from RBS experiments.

The RBS and nuclear reaction analysis (NRA) channelling experiments were carried out using the 2 MV Van de Graaff beam facility of the LNETI at Sacavém. The RBS experiments were performed with 1.6 MeV H^+ and He^+ particles. Typical currents of 1 nA were applied in order to keep the beam-induced damage low. Simultaneously with the H^+ RBS channelling analysis the $^7Li(p,\alpha)^4He$ nuclear reaction was used in order to obtain information about the Li position. The spectra of the H^+ and He^+ back-scattered particles detected with a surface barrier detector with a resolution of 14 keV placed at 140° to the beam direction were collected in a multichannel analyser where windows could select the signals from niobium, oxygen and heavy dopants. An annular surface barrier detector placed at 180° with the incident beam direction was used to accumulate the α-particles of the $^7Li(p,\alpha)^4He$ nuclear reaction. The energy resolution was 18 keV.

Table 2. Concentrations of the dopants determined by the AAS or ICP methods and the positions of the OH absorption bands in Mg^{2+}-and-M^{3+}-co-doped $LiNbO_3$ crystals. R is the ratio of the amount of M^{3+} involved in the Mg–OH–M defect complex to the total M^{3+} concentration.

Spectrum in figure 8	Dopant	Mg concentration (mol%)		Dopant concentration (mol%)		OH wavenumber (cm^{-1})	Integral absorption (cm^{-2})	R (%)	Remark
		Melt	Crystal	Melt	Crystal				
A	In	6	5.9	1	0.59	3484.6			Weak OH
						3507.0	30.6	1	Mg–OH–M
						3527.7			Mg–OH
						3538.6			Mg–OH
B	Sc	6	6.1	1	0.95	3507.4	42.4	1	Mg–OH–M
						3527.7			Mg–OH
						3538.1			Mg–OH
C	Lu	6	5.2	1	0.76	3482.5			Weak OH
						3499.1	15.2	0.5	Mg–OH–M
						3529.2			Mg–OH
						3538.6			Mg–OH
D	Nd	6	6.5	2	0.14	3522.5	10.8	2	Mg–OH–M
						3527.8			Mg–OH
						3538.0			Mg–OH
E	Nd	6	6.5	0.5	0.03	3522.1	9.3	8	Mg–OH–M
						3527.4			Mg–OH
						3537.6			Mg–OH

The PIXE channelling experiments were performed using a 1.5 MeV proton beam obtained from the CNRS 4 MV Van de Graaff accelerator in Strasbourg. The PIXE spectra were recorded with an Si(Li) x-ray detector with an energy resolution of 180 eV placed at an angle of 150° with respect to the incident beam direction. Windows were set in the x-ray spectrum corresponding to the L lines of Nb and the dopants under investigation (In and Nd). The angular scans were taken at room temperature. A fresh beam spot on the crystal was chosen after each angular scan to avoid radiation damage. When performing the angular scans, care was taken to include background corrections and pile-up effects.

A comparison of the angular dependence of the normalized yields with either the Nb or the Li signals gives information about the lattice site location of the dilute dopants. Because of the low sensitivity of the RBS technique for detecting Mg in $LiNbO_3$ and the low energy of the x-ray signals of Mg in the PIXE experiments, direct information on the lattice site of Mg could not be obtained in this work.

The plate-like samples used in RBS and PIXE experiments were cut either perpendicular or parallel to the c axis. They were mechanically polished and chemically etched in a mixture of 1:2 parts of HF and HNO_3.

The IR absorption spectra of the OH^- vibrations were measured with a Hitachi double-beam IR or a Perkin–Elmer 1710 FTIR spectrophotometer at room temperature. The spectra were generally recorded using unpolarized light propagating parallel to the crystallographic c axis. In order to determine the direction of the OH^- dipole, polarized light was used, obtained from a Perkin–Elmer wire-grid polarizer having about 98% efficiency in the given wavenumber range. The OH^- absorption was then measured using incident light propagating perpendicular to the c axis while the electric field vector was rotated around the propagation direction.

3. Crystal structure

At room temperature the ferroelectric $LiNbO_3$ belongs to the $R3c$ trigonal (rhombohedral) space group; the point group is $3m$ (see, e.g., [1, 20]). In trigonal systems, hexagonal unit cells are usually chosen and conventionally characterized by four Miller indices $(hkil)$ corresponding to three equivalent a axes 120° apart, lying in a plane normal to the trigonal c axis, while the fourth index belongs to c. The a axes are chosen to be perpendicular to the mirror planes of symmetry. In this paper we use this conventional hexagonal notation.

In $LiNbO_3$ the hexagonal unit cell contains six formula units. Perpendicular to the c axis, oxygen atoms are placed in a hexagonal close-packed structure. The slightly distorted oxygen octahedra sharing faces along the trigonal c axis contain cations in the order Li, Nb, empty, Li, Nb, empty, ... (figure 1). The empty octahedron is often called a structural or intrinsic vacancy. The cation sites as well as the free octahedral sites are generally indistinguishable from symmetry considerations as all of them have trigonal symmetry.

4. Results

4.1. RBS and PIXE channelling

Figure 2 shows the angular scans of the normalized yield of Nb and Li signals along

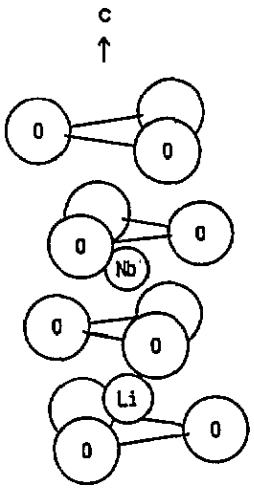

Figure 1. The oxygen octahedra filled with Li and Nb, and the structurally free octahedron, along the crystallographic *c* axis.

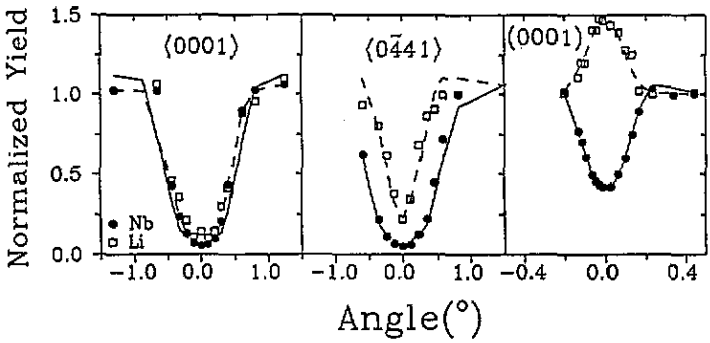

Figure 2. The angular scans of the back-scattered protons and emitted α-particles from niobium (●) and lithium (□), respectively, along two axial and the (0001) planar directions: ——, yields for Nb obtained from computer simulation; – – –, yields for Li obtained from computer simulation.

two 'axial' directions and one 'planar' direction, corresponding to one- and two-dimensional channels, respectively, in the crystal. The full circles and open squares represent the Nb and Li yields, respectively, observed experimentally. The full and broken curves represent a computer simulation described elsewhere [36]. These scans can be qualitatively understood taking into account the projections shown in figure 3. Along the ⟨0001⟩ direction, Li atoms are shadowed by Nb atoms, which explains the essentially identical angular scans for Li and Nb signals. This is not the case along the ⟨0$\bar{4}$41⟩ direction where Li atoms are slightly dislocated from Nb atoms, in good agreement with the observation of a narrow dip. Along the *c* plane the broad flux peak observed is qualitatively explained by the central position of the Li atoms between the Nb and O layers as has been discussed in [14].

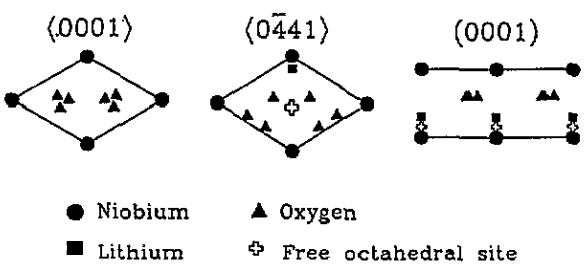

Figure 3. Projections of the lattice sites of $LiNbO_3$ on planes normal to the indicated directions.

Figure 4 shows results corresponding to the lattice site locations of Er and Lu, figure 5 the corresponding results for In and Nd, and figure 6 the corresponding

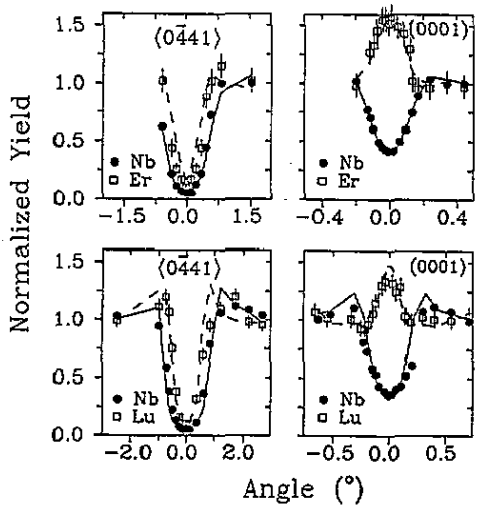

Figure 4. The angular scans of back-scattered protons from erbium (□, upper figures) and of back-scattered α-particles from lutetium (□, lower figures) compared with niobium (●) in $LiNbO_3$:Mg crystals, for the ⟨0441⟩ axial and (0001) planar directions: ——, calculated yields for Nb obtained from computer simulation; – – –, yields calculated assuming 100% Er at Li sites (upper figures) and 90% Lu at Li sites and 10% Lu at Nb sites (lower figures).

results for Gd and Tm atoms. The full and broken curves represent again the yields from Nb and the dopant, respectively, calculated using the computer simulation. In figure 4 the flux peak of back-scattered protons from Er atoms along the *c* plane gives about the same yield as that for the Li shown in figure 2. This clearly indicates that the Er atoms occupy Li sites. The angular scan for Er along the ⟨0441⟩ direction shows a broad dip, reflecting the fact that Er atoms are shadowed by Li. We draw attention to the excellent agreement between the measured data and the results calculated by assuming 100% substitution of Er for Li.

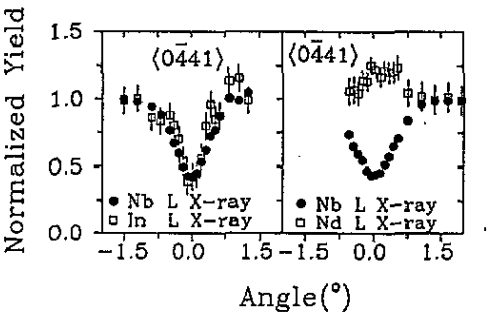

Figure 5. The angular scans for emitted L x-ray lines from indium (□, left) and neodymium (□, right) compared with the niobium signals (●) in $LiNbO_3$:Mg crystals along the ⟨0441⟩ axial direction.

Similar behaviour is observed with Lu atoms (figure 4); however, the flux peak along the (0001) planar direction is not so high. This indicates that not all Lu ions

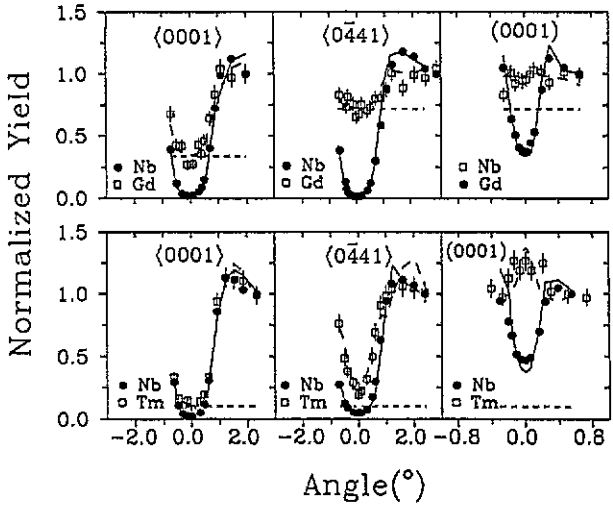

Figure 6. The angular dependence of the back-scattered α-particles from gadolinium (□, upper figures) and thulium (□, lower figures) compared with niobium (●) in $LiNbO_3$:Mg crystals for the ⟨0001⟩ and ⟨0$\bar{4}$41⟩ axial and (0001) planar directions: ——, yields calculated for Nb; – – –, yields for Tm and Gd calculated by computer simulation assuming site occupancy as described in the text. The horizontal broken lines show the fraction of the dopants assumed to be in the random position.

occupy Li sites. In the angular scan for the ⟨0001⟩ axis, not included in the figure, the dip for Lu coincides exactly with that for Nb, suggesting that Lu atoms are shadowed by Nb atoms. The angular scan along the ⟨0$\bar{4}$41⟩ axis excludes the free octahedral site. Thus the simulation was performed taking into account a small fraction of Lu at the Nb site and resulted in good agreement with the experimental data.

The energy resolution of the RBS technique did not allow us to use that method for In, because the atomic mass of In is close to that of Nb. The results obtained for indium with the PIXE technique (figure 5) are also in good agreement with the Li site occupation; however, the sensitivity of the technique is not good enough to say that all In atoms occupy Li sites. Thus we may conclude that most In atoms substitute for Li atoms, while a small fraction of these impurities may occupy other (e.g. Nb) sites.

The concentration of Nd actually present in the crystal (see table 2) was too low to use the RBS method. The sensitivity of the PIXE technique was, however, good enough to show that the lattice site occupation of Nd is different from that of Er, In and Lu. The flux peak in the ⟨0$\bar{4}$41⟩ direction (figure 5) supports the conclusion that some of the Nd atoms occupy empty octahedral sites. However, the results available (see also [35]) also show that a significant number of Nd probably occupy other sites including, for example, Nb. Computer simulation cannot be done for PIXE results at present. To understand the physics of the PIXE measurements the reader can find more details in [14].

In the case of Tm the flux peak in the c plane (figure 6) indicates that a large fraction occupy Li sites. However, since the minimum yield along the ⟨0001⟩ direction does not overlap with that for Nb, none of the regular octahedral positions mentioned up to now can explain the results. However, randomly displaced positions inside the Li and/or Nb octahedra may explain the results. This 'random' fraction is estimated

to be not larger than 10%. Similarly to Lu we cannot exclude the presence of a small number of Tm atoms at Nb sites—up to 10%. The simulations were performed with 80% of Tm at Li sites, 10% at Nb sites and 10% at 'random' positions, showing good agreement with the experimental data.

The behaviour of Gd is very similar to that of Tm, although the percentage of randomly distributed Gd ions seems to be higher. In the faces normal and parallel to the ⟨0001⟩ axis, the 'random' fractions were about 34% and 72%, respectively. The remaining Gd ions are found to occupy Li sites.

Table 3 summarizes the conclusions drawn for the dopants studied by the RBS and PIXE channelling techniques and using the computer simulation method.

Table 3. Summary of lattice sites for the dopants in $LiNbO_3$:Mg crystals based on RBS and PIXE results. The 'random' lattice sites include those possibly incorporated into various aggregates, e.g. self-compensated M_{Li}–M_{Nb} pairs. The dopants In and Nd were measured by the PIXE technique, for which no quantitative conclusions can be drawn for lack of a computer simulation. The position occupied by Nd ions is still an unsolved problem. A fraction, however, seem to occupy the free octahedral site.

	Amount (%)			
	Li octahedron	Nb octahedron	Free octahedron	'Random' position
In	Mainly			
Nd			Partly	
Gd	≃30			≃ 70
Er	100	—	—	—
Tm	>80	< 10	—	≃ 10
Lu	>90	< 10	—	—

4.2. IR absorption spectra

The IR absorption spectra of OH^- vibrations in $LiNbO_3$:Mg,M^{3+} (M ≡ Y, Er, Tm, Gd, In, Sc, Lu, Nd) crystals measured at room temperature are shown in figures 7 and 8. Relatively broad (10–30 cm^{-1}) OH^- bands were found in the 3480–3540 cm^{-1} wavenumber range. No marked improvement can be achieved in the resolution by cooling the crystals to a low temperature. A decomposition procedure by the least-squares method (described in detail in [27]) has been performed in order to separate the band components. The wavenumbers of the components found in doubly doped $LiNbO_3$ are listed in tables 1 and 2.

Three kinds of OH^- band can be observed in the doubly doped crystals. First, at high energies there are two components at about 3528 and 3538 cm^{-1} which have been attributed to hydroxyl vibrations in Mg–OH complexes [29]. These two components are present in each sample as expected for crystals containing about 5 mol% Mg or more. Second, weak bands at around 3485 and 3495 cm^{-1} seem to appear in most of the samples corresponding to the well known OH^- bands always present in nominally pure or weakly doped $LiNbO_3$ crystals [27]. The appearance of the bands reveals that the Mg concentration in the crystals is only slightly above the threshold. When the Mg concentration is increased to 8 mol% in the Y- or Er-doped $LiNbO_3$ crystal, the bands at about 3490 cm^{-1} disappear (compare curves A and B or curves C and D in figure 7) and only the 3528–3538 cm^{-1} two-component bands

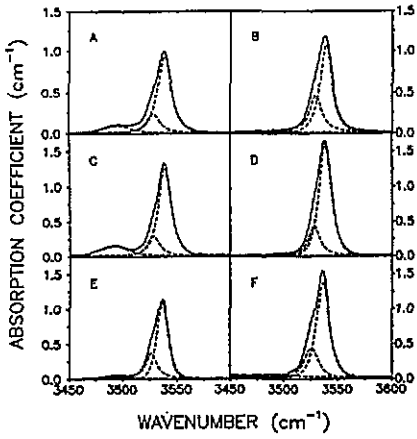

Figure 7. The IR absorption bands of OH^- ions in $LiNbO_3$:Mg crystals co-doped with yttrium (curves A and B), erbium (curves C and D), thulium (curve E) and gadolinium (curve F). See also table 1.

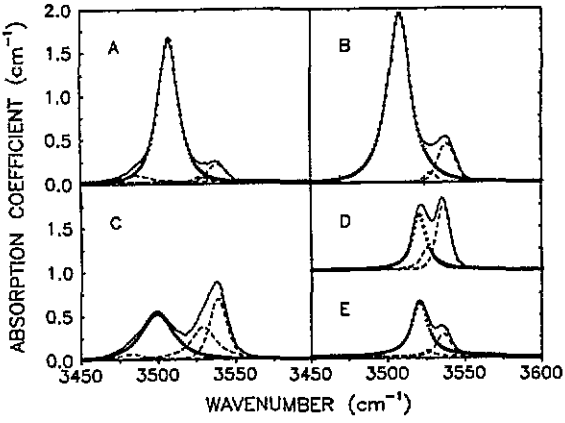

Figure 8. The IR absorption bands of OH^- ions in $LiNbO_3$:Mg crystals co-doped with indium (curve A), scandium (curve B), lutetium (curve C) and neodymium (curves D and E). See also table 2.

remain as expected. Finally, a third kind of OH^- absorption band between 3499 and 3523 cm^{-1} can be observed in samples doped with In, Sc, Lu and Nd (figure 8, dotted curves). The bands found in the Nd-, Lu- and In-doped crystals have already been presented elsewhere [33, 35], but the band in the Mg-and-Sc-co-doped crystal is shown here for the first time. These bands have been attributed to hydroxyl vibrations in some kind of Mg–OH–M defect complex since they are only present in doubly doped crystals [33, 35].

In order to discover more about the orientation of the OH^- ions involved in the Mg–OH–M defect the polarized spectra of the OH^- absorption have also been measured. Figure 9 shows the dependence of the absorption coefficient on the angle θ of polarization for the maxima at 3507 and 3538 cm^{-1} of the Mg-and-In-co-doped $LiNbO_3$ crystal. θ represents the angle between the electric field vector of the IR radiation and the oxygen plane perpendicular to the c axis. The absorbance $A(\theta)$ of a sample with a thickness d can be written as

$$A(\theta) = -\ln[\exp(-\alpha_X d)\cos^2\theta + \exp(-\alpha_Z d)\sin^2\theta] \tag{1}$$

where α_X and α_Z are the absorption coefficients for light polarized along the X axis and Z axis, respectively [37]. In our notation, X corresponds to the a_1 axis while Z is identical with c. The full curve fitted to the experimental data in figure 9 represents the $A(\theta)$ function calculated from equation (1).

The directions of the OH^- dipoles contained in the Mg–OH–M and Mg–OH complexes can be estimated from the ratios of the maxima to minima of the curves belonging to the 3507 and 3538 cm^{-1} transitions, respectively:

$$D = \alpha_X/\alpha_Z \simeq \tfrac{1}{2}\cot^2\chi \tag{2}$$

where χ is the angle between the OH^- dipole moment and the oxygen plane perpendicular to the c axis. For the Mg–OH complex the maximum-to-minimum ratio

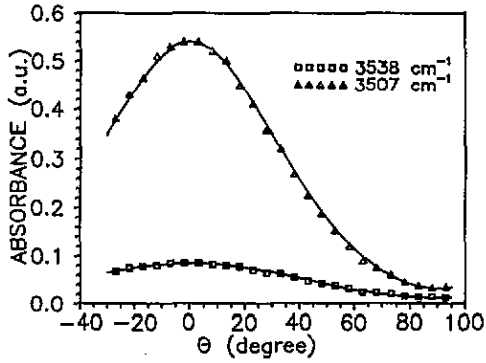

Figure 9. The polarization dependence of the OH^- bands at 3507 and 3538 cm^{-1} in an $LiNbO_3$:Mg,In crystal. θ represents the angle between the electric field vector of the incident beam and the oxygen plane perpendicular to the c axis.

was found to be 7 corresponding to about 15°, which is in rather good agreement with the value measured for $LiNbO_3$ doped with only Mg [29]. The angle χ between the c plane and the OH^- dipole for the Mg–OH–In complex calculated from the maximum-to-minimum ratio of about 17 is equal to about 10°. At high D-values some correction has to be taken into account related to the efficiency of the IR polarizer used [38]. On the assumption of a polarization efficiency of 98% at our wavenumbers the angle χ is estimated to be as low as $5 \pm 5°$; so the direction of the OH^- dipole moment is very close to the c plane.

5. Discussion

Let us first discuss the origin of the third type of OH^- IR band between 3499 and 3523 cm^{-1} (see figure 8 and table 2). These bands appear only in the In-, Sc-, Lu- or Nd-co-doped samples, which supports the interpretation in terms of an Mg_{Li}–OH_O–M_{Nb} complex defect (where the subscripts represent substitution sites) suggested previously for Cr-, Fe- or Nd-co-doped samples [30, 32, 33].

There are two kinds of close neighbour pair of Nb and Li sites in the crystal. The distance between neighbouring Nb and Li sites along the c axis is 0.3064 nm. A very similar (0.3068 nm) distance between Nb and Li ions is present nearly perpendicular to the c axis as well. The OH^- ion substituting for oxygen is assumed to be located between the two cations. The OH^- dipole moment lying nearly in the c plane, as obtained for the Mg-and-In-co-doped crystal, is consistent with the assumption that the magnesium and the trivalent dopant are placed along the c axis. Otherwise the direction of the O–H bond would strongly deviate from the c plane, contradicting the polarization dependence measurements.

From the intensities of the third type of IR band we estimated the concentrations of OH^- ions involved in various Mg–OH–M defects. This way the percentage of trivalent dopants forming defect complexes with magnesium and hydroxyl ions can also be obtained. Values of the integral absorption

$$I = \int \alpha(\nu)\, \mathrm{d}\nu \tag{3}$$

of the bands attributed to Mg–OH–M complexes are listed in table 2, where α is the absorption coefficient and ν is the wavenumber. Using a recent calibration for

the absorption strength a per ion, for OH^- ($a \simeq 9 \times 10^{-18}$ cm [39]), the OH^- concentration equals

$$n = I/a \ln 10 \tag{4}$$

and consequently the number of M^{3+} ions involved in the Mg–OH–M defect can be calculated. The ratio R of this number to the total M^{3+} concentration is also shown in table 2. The low values of R indicate that only a small portion of the trivalent dopants form defect complexes with magnesium and hydroxyl ions.

It should be mentioned that a number of different calibrations can be found in the literature for the concentration of OH^- ions in oxide crystals. They differ by about two orders of magnitude, as is discussed in detail in [39]. The calibration used here is based on proton-exchanged $LiNbO_3$ crystals where the degree of lithium–proton exchange is well determined by the lithium content of the benzoic acid used for the exchange process. Then the absorption strength per ion can easily be calculated by measuring the IR absorption of OH^- ions and dividing the integral absorption by the number of protons. A previous calibration [33] for the OH^- absorption used in [35] gave an absorption strength lower by approximately one order of magnitude, resulting in higher R-values. That calibration was based on an assumption that all Cr^{3+} ions form Mg–OH–M complexes in $LiNbO_3$: Mg, Cr crystals [33]. If this assumption were valid for other trivalent dopants, much higher OH^- absorptions should have been found for Sc-, In- or Lu-doped $LiNbO_3$:Mg crystals where the concentration of the trivalent dopants was between 0.5 and 1 mol% (table 2), i.e. more than an order of magnitude larger than the Cr concentration used in [30]. Even if we assume that the calibration based on the OH^- absorption of the proton-exchanged layer is not strictly valid for the Mg–OH–M complexes, a factor of 2 or 3 in the absorption strength value does not change significantly the conclusion that only a small portion of Sc, In or Lu form Mg–OH–M defects.

In the case of Er, Y, Tm and Gd, no absorption band related to the Mg–OH–M defect was observed (see figure 7). Since the trivalent dopant in the defect complex is assumed to substitute for niobium, it is straightforward to assume that these ions do not even partially occupy niobium positions in the crystal lattice. This assumption was confirmed by the RBS channelling experiments for erbium which was found only on lithium sites.

For Tm and Gd, comparison with RBS data is less straightforward, given the appreciable fraction of these dopants which occupy unidentified (random) positions in the lattice. One can conclude only that Tm and Gd in these positions are not available for the formation of Mg–OH–M complexes. Accordingly either these ions may be at modified Li positions or, if they are still inside Nb octahedra, they must be constituents of another type of complex defect such as self-compensating M_{Li}–M_{Nb} pairs. In the latter case a number of nearly equivalent configurations are possible, which might explain the failure that for the given fractions no well defined sites could be derived.

Lu and In atoms in $LiNbO_3$:Mg crystals were also found mainly on lithium sites. It is clearly seen from the RBS and PIXE channelling experiments that a small fraction of these impurities may occupy niobium sites as well. This means that a small portion of Lu and In ions may form Mg_{Li}^{2+}–OH_O^-–M_{Nb}^{3+}-type defects in agreement with table 2, where 0.5–1% of the dopants was estimated to be present in that complex.

According to the PIXE data a fraction of neodymium atoms seem to occupy the structurally empty oxygen octahedra in the $LiNbO_3$:Mg crystal. This may be related

to the large ionic radius and the low distribution coefficient of Nd (see table 2). These results do not exclude, however, that some Nd ions substitute for host cations. According to our IR results, partial substitution for Nb should also be possible as 2–8% of Nd should form Mg–OH–M defects. It should be pointed out that, in $LiNbO_3$ crystals containing no Mg, the RBS results show that Nd ions occupy Li octahedra at an appreciable displacement from the Li site [18].

$LiNbO_3$:Mg crystals co-doped with Y or Sc ions were studied only by the IR absorption method. Chemical analysis shows that both Y and Sc ions are incorporated into the crystal and their distribution coefficients are close to 1. Similarly to most of the trivalent dopants we expect them to substitute mainly for lithium ions. We assume further that several per cent of scandium substitutes for niobium as well, since the crystal showed an OH^- band at about 3507 cm^{-1}, which is attributed to an OH^- vibration in the Mg_{Li}^{2+}–OH_O^-–Sc_{Nb}^{3+} defect complex.

6. Conclusion

The RBS and PIXE channelling techniques and the IR absorption spectroscopy method have provided complementary information on the incorporation of the trivalent dopants into $LiNbO_3$ crystals co-doped with magnesium.

The channelling techniques showed that most trivalent dopants investigated, namely In, Er, Tm and Lu, preferentially occupy Li sites, while for Gd the same may be true if the unidentified portion is due to self-compensated pairs. Although the conclusion about the preference for Li substitution refers to $LiNbO_3$:Mg crystals, it is felt to hold also for $LiNbO_3$ containing no Mg, since Mg is assumed to compete for Li sites. For Nd, partial substitution at empty octahedral sites cannot be excluded.

The IR absorption measurements were sensitive to small fractions of dopants substituting for niobium. So, in the case of Sc, In, Nd and Lu a small portion of the dopants were found to substitute for niobium as shown by the formation of Mg_{Li}^{2+}–OH_O^-–M_{Nb}^{3+} complex defects. In this complex the magnesium and the trivalent dopant are assumed to occupy neighbouring Li and Nb sites, respectively, along the trigonal c axis while the hydroxyl ion is located in the oxygen plane between the cations.

Acknowledgments

Financial support from the National Science Fund of Hungary (OTKA grants 23 and T4420), the Junta Nacional de Investigacao Cientifica e Tecnológica of Portugal for a PhD grant from Programa Ciencia (LR) and the Comision Interministerial de Ciencia y Tecnologia of Spain is acknowledged. This work has been partially performed under a NATO grant (CRG.890934) for collaborative research. The authors are grateful to I Cravero and O Szakács for the impurity analysis and to B Zelei for some of the IR absorption measurements.

References

[1] Räuber A 1978 *Current Topics in Materials Science* vol 1, ed E Kaldis (Amsterdam: North-Holland)
[2] 1989 *Properties of Lithium Niobate (EMIS Datareviews Series 5)* (London: INSPEC, IEE)

[3] Nassau K 1967 *Ferroelectricity* ed E F Weller (Amsterdam: Elsevier)
[4] Corradi G, Söthe H, Spaeth J M and Polgár K 1990 *J. Phys.: Condens. Matter* **2** 6603
[5] Zaldo C, Agulló-López F, García J, Marcelli A and Mobilio S 1989 *Solid State Commun.* **71** 243
[6] Rebouta L, Soares J C, da Silva M F, Sanz-García J A, Diéguez E and Agulló-López F 1991 *Nucl. Instrum. Methods* B **50** 428
[7] Prieto C, Zaldo C, Fessler P, Dexpert H, Sanz-García J A and Diéguez E 1991 *Phys. Rev.* B **43** 2594
[8] Zaldo C, Prieto C, Dexpert H and Fessler P 1991 *J. Phys.: Condens. Matter* **3** 4135
[9] Corradi G, Söthe H, Spaeth J-M and Polgár K 1991 *J. Phys.: Condens. Matter* **3** 1901
[10] Martín A, López F J and Agulló-López F 1992 *J. Phys.: Condens. Matter* **4** 847
[11] Grachev V G, Malovichko G I and Troitskii V V 1987 *Sov. Phys.–Solid State* **29** 349
[12] Jia Weiyi, Liu Huimin, Knutson R and Yen W M 1990 *Phys. Rev.* B **41** 10 906
[13] Shiu G G and Zhao Min-Guang 1991 *Phys. Rev.* B **43** 13 575
[14] Rebouta L, da Silva M F, Soares J C, Hage-Ali M, Stoquert J P, Siffert P, Sanz-García J A, Diéguez E and Agulló-López F 1991 *Europhys. Lett.* **14** 557
[15] Catlow C R A, Chadwick A V, Cole M and Tomlinson S M 1991 *Radiat. Eff. Defects Solids* **119** 565
[16] Arizmendi L, Abella F and Cabrera J M 1984 *Ferroelectrics* **56** 75
[17] Lifante G, Cussó F, Jaque F, Sanz-García J A, Monteil A, Varrel B, Boulon G and García-Solé J 1991 *Chem. Phys. Lett.* **176** 482
[18] Rebouta L, Soares J C, da Silva M F, Sanz-García J A, Diéguez E and Agulló-López F 1992 *Mater. Res. Soc. Symp. Proc.* vol 244 (Pittsburgh, PA: Materials Research Society) p 311
[19] Donnerberg H, Tomlinson S M, Catlow C R A and Schirmer O F 1991 *Phys. Rev.* B **44** 4877
[20] Abrahams S C and Marsh P 1986 *Acta Crystallogr.* B **42** 61
[21] Donnerberg H, Tomlinson S M, Catlow C R A and Schirmer O F 1989 *Phys. Rev.* B **40** 11 909
[22] Polgár K, Kovács L, Földvári I and Cravero I 1986 *Solid State Commun.* **59** 375
[23] Zhong Gi-Guo, Jin Jian and Wu Zhong-Kang 1980 *Proc. 11th Int. Quantum Electronics Conf.* (New York: IEEE) p 631
[24] Rebouta L, da Silva M F, Soares J C, Sanz-García J A, Diéguez E and Agulló-López F 1992 *Nucl. Instrum. Methods* B **64** 189
[25] Böker A, Donnerberg H, Schirmer O F and Feng Xiqi 1990 *J. Phys.: Condens. Matter* **2** 6865
[26] Camarillo E, Tocho J, Vergara I, Diéguez E, García-Solé J and Jaque F 1992 *Phys. Rev.* B **45** 4600
[27] Kovács L, Wöhlecke M, Jovanovic A, Polgár K and Kapphan S 1991 *J. Phys. Chem. Solids* **52** 797
[28] Bryan D A, Gerson R and Tomaschke H E 1984 *Appl. Phys. Lett.* **44** 847
[29] Kovács L, Polgár K and Capelletti R 1987 *Cryst. Latt. Defects Amorph. Mater.* **15** 115
[30] Kovács L, Földvári I, Cravero I, Polgár K and Capelletti R 1988 *Phys. Lett.* **133A** 433
[31] Feng Xi-Qi, Ying Ji-Feng, Wu Yao-An and Liu Jian-Cheng 1991 *Chinese Sci. Bull.* **36** 297
[32] Wang Hong, Wen Jinke, Li Bin and Wang Huafu 1990 *Phys. Status Solidi* a **118** K47
[33] Kovács L, Szaller Zs, Cravero I, Földvári I and Zaldo C 1990 *J. Phys. Chem. Solids* **51** 417
[34] Kovács L, Rebouta L, Soares J C and da Silva M F 1991 *Radiat. Eff. Defects Solids* **119** 445
[35] Kovács L, Rebouta L, Soares J C, da Silva M F, Hage-Ali M, Stoquert J P, Siffert P, Zaldo C, Szaller Zs and Polgár K 1991 *Mater. Sci. Eng.* B **9** 505
[36] Rebouta L, Smulders P, Boerma D, Agulló-López F, da Silva M F and Soares J C 1993 *Phys. Rev.* B at press
[37] Turrell G 1972 *Infrared and Raman Spectra of Crystals* (London: Academic)
[38] Zbinden R 1964 *Infrared Spectroscopy of High Polymers* (New York: Academic)
[39] Klauer S, Wöhlecke M and Kapphan S 1992 *Phys. Rev.* B **45** 2786